GTP Cyclohydrolase 1/Tetrahydrobiopterin Counteract Ferroptosis through Lipid Remodeling

Vanessa A. N. Kraft,[†,◆] Carla T. Bezjian,[‡,◆] Susanne Pfeiffer,[†,◆] Larissa Ringelstetter,[§] Constanze Müller,[‖] Fereshteh Zandkarimi,[⊥] Juliane Merl-Pham,[#] Xuanwen Bao,[▽] Natasa Anastasov,[▽] Johanna Kössl,[†] Stefanie Brandner,[§] Jacob D. Daniels,[○] Philippe Schmitt-Kopplin,[‖] Stefanie M. Hauck,[#] Brent R. Stockwell,[*,‡,⊥] Kamyar Hadian,[*,§] and Joel A. Schick[*,†]

[†]Institute of Molecular Toxicology and Pharmacology, Genetics and Cellular Engineering Group, HelmholtzZentrum Muenchen, Ingolstaedter Landstr. 1, 85764 Neuherberg, Germany

[‡]Department of Chemistry, Columbia University, 550 West 120th Street, MC4846, New York, New York 10027, United States

[§]Institute of Molecular Toxicology and Pharmacology, Assay Development and Screening Platform, HelmholtzZentrum Muenchen, Ingolstaedter Landstr. 1, 85764 Neuherberg, Germany

[‖]Research Unit Analytical BioGeoChemistry, HelmholtzZentrum Muenchen, Ingolstaedter Landstr. 1, 85764 Neuherberg, Germany

[⊥]Department of Biological Sciences, Columbia University, New York, New York 10027, United States

[#]Research Unit Protein Science, HelmholtzZentrum Muenchen, Ingolstaedter Landstr. 1, 85764 Neuherberg, Germany

[▽]Institute of Radiation Biology, HelmholtzZentrum Muenchen, Ingolstaedter Landstr. 1, 85764 Neuherberg, Germany

[○]Department of Pharmacology, Columbia University, New York, New York 10027, United States

S *Supporting Information*

ABSTRACT: Ferroptosis is an iron-dependent form of regulated cell death linking iron, lipid, and glutathione levels to degenerative processes and tumor suppression. By performing a genome-wide activation screen, we identified a cohort of genes antagonizing ferroptotic cell death, including GTP cyclohydrolase-1 (GCH1) and its metabolic derivatives tetrahydrobiopterin/dihydrobiopterin (BH_4/BH_2). Synthesis of BH_4/BH_2 by GCH1-expressing cells caused lipid remodeling, suppressing ferroptosis by selectively preventing depletion of phospholipids with two polyunsaturated fatty acyl tails. GCH1 expression level in cancer cell lines stratified susceptibility to ferroptosis, in accordance with its expression

in human tumor samples. The GCH1-BH_4-phospholipid axis acts as a master regulator of ferroptosis resistance, controlling endogenous production of the antioxidant BH_4, abundance of CoQ_{10}, and peroxidation of unusual phospholipids with two polyunsaturated fatty acyl tails. This demonstrates a unique mechanism of ferroptosis protection that is independent of the GPX4/glutathione system.
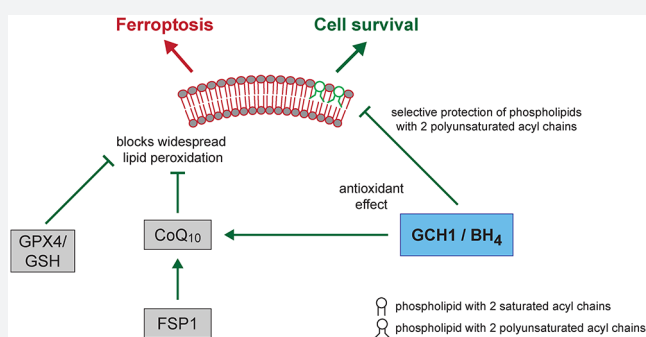
INTRODUCTION

Ferroptosis is a form of regulated cell death that results from alterations in iron and glutathione homeostasis, leading to lethal lipid peroxidation.[1−3] Loss of capacity to repair lipid peroxides can result in cellular demise.[4−6] To date, four classes of ferroptosis inducers have been described (i.e., erastin, RSL3, FIN56, and $FINO_2$) that ultimately cause loss of cellular GPX4 activity and accumulation of phospholipid hydroperoxides, which drive cell death.[3,7−9] Conversely, phospholipid hydroperoxide removal, catalyzed by GPX4, supports cellular homeostasis and viability against otherwise lethal stresses.[10] A reduced threshold of peroxidation-susceptible phospholipid substrates, iron depletion, lipophilic antioxidants, or treatment with the radical trapping antioxidants ferrostatin-1 or

liproxstatin-1 suppresses ferroptotic cell death.[1,11,12] Ferroptosis has been implicated in degenerative pathologies, including neurodegenerative disorders, ischemic injuries, and heat stress in plants, among other processes.[2]

Mammalian cells have evolved distinct mechanisms to cope with increased levels of oxidative damage.[13−15] One metabolic pathway frequently implicated in production of reactive oxygen species includes GCH1/tetrahydrobiopterin, where GCH1 (GTPCH) is the rate-limiting enzyme for $6(R)$-L-erythro-5,6,7,8-tetrahydrobiopterin (BH_4) synthesis.[16,17] BH_4, in the presence of iron in enzyme catalytic sites, is a requisite cofactor
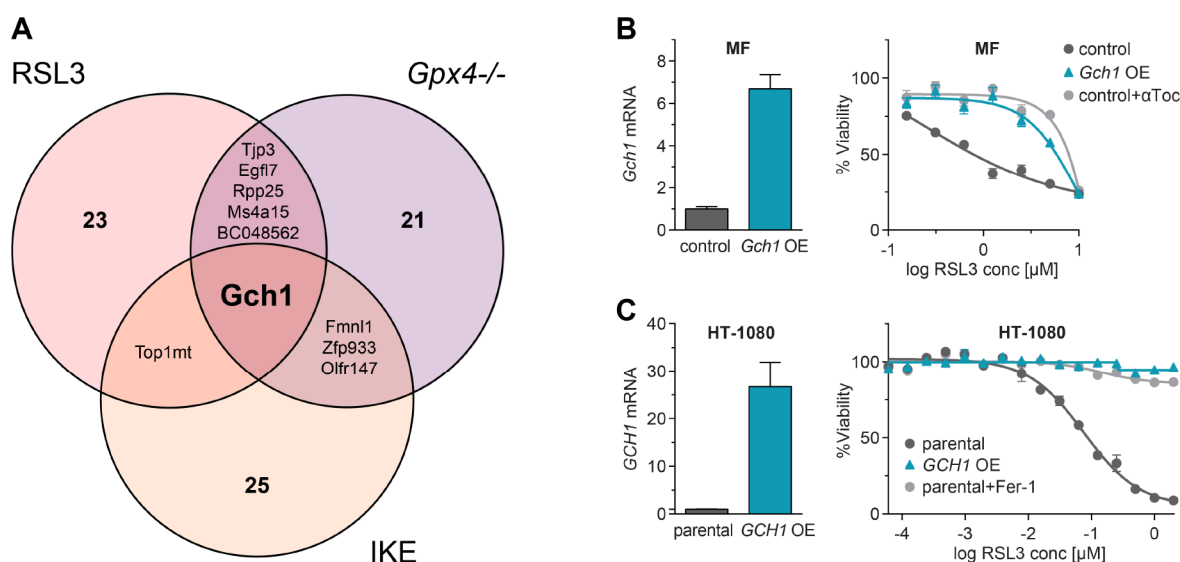
Figure 1. A CRISPR activation screen identifies *Gch1* as ferroptosis antagonist. (A) Venn diagram of overlapping top 30 genes found in each overexpression screen against ferroptosis inducers 0.3 μM RSL3, 2 μM IKE, and *Gpx4−/−* by 1 μM tamoxifen. (B) Relative *Gch1* mRNA expression levels and dose response curves against RSL3 treatment in *Gch1*-overexpressing MF-dCas9-*Gch1* (*Gch1* OE) cells and empty vector control (control) immortalized mouse fibroblasts. Addition of 10 μM α-tocopherol (αToc) serves as rescue control for ferroptosis. (C) Relative *GCH1* mRNA expression levels and dose response curve against RSL3 treatment in HT-1080 cells overexpressing *GCH1*-IRES-Puro construct (*GCH1* OE) and parental HT-1080 cells (parental) $\pm$ 2 μM ferrostatin-1 (Fer-1) rescue. Viability data are plotted as mean $\pm$ SEM of $n = 3$ (B) or $n = 2$ (C) technical replicates of at least three repetitions of the experiment with similar outcomes. Relative mRNA expression is shown as mean $\pm$ SD of $n = 3$ technical replicates of three independent repetitions of the experiment with similar results.

for production of aromatic amino acids, neurotransmitters, and nitric oxide. Withdrawal of BH_4 can lead to uncoupling of nitric oxide synthases (NOSs) and superoxide generation.[18] Notably, GCH1 activity is negatively regulated by a feedback loop triggered by increased BH_4 via GCHFR, the GTP cyclohydrolase I feedback regulator.[19]

In humans, *GCH1* is a polymorphic locus important for pain sensitivity, cardiovascular risk, and DOPA-responsive dystonia, among other afflictions.[16,20−25] Furthermore, *GCH1* alternations are manifested in chronic diseases, including hypertension, diabetes, and arthrosclerosis,[20,21] and are implicated in Parkinson's disease.[22,26] Several studies also point toward a role for GCH1 in some cancers.[27−29]

To identify additional pathways controlling ferroptosis susceptibility, we performed a CRISPR/dCas9 overexpression screen using a genome-wide activation library. Elevated gene expression, as opposed to gene knockout, is less impacted by functional redundancy and can uncover mechanisms governing cell survival. Using this method, we identified a set of protective genes that suppress ferroptosis, most prominently GCH1. Metabolic analysis of *GCH1*-overexpressing cells revealed BH_4/BH_2 as the source of the potent antiferroptotic effect of GCH1 overexpression. Supplementation with either substance rescued cell viability. Moreover, *GCH1* modulation by overexpression or knockdown rendered cancer cells correspondingly resistant or sensitive to ferroptotic cell death in cultured cells. Strikingly, lipidomics analysis showed *GCH1*-overexpressing cells have protected phosphatidylcholine phospholipids with two polyunsaturated fatty acyl (PUFA) chains and enrich amounts of reduced CoQ_{10} levels after ferroptosis induction, for example, upon IKE treatment. These results illuminate a potent new axis of resistance for countering ferroptosis by an endogenously produced antioxidant and introduce a new lethal lipid oxidation product as a driver of ferroptosis in these contexts.

RESULTS

A Whole-Genome Activation Screen Identifies GCH1 as a Potent Antagonist of Ferroptosis. To identify genes protecting against ferroptosis, we chose three established ferroptosis inducers: (1S, 3R)-RSL3 (henceforth RSL3), imidazole ketone erastin (IKE), and genetic ablation of *Gpx4*. For the latter, we took advantage of a tamoxifen-inducible *Gpx4* knockout system in immortalized murine fibroblast (MF) cells.[30] We employed a genome-wide dCas9-based activation screen (CRISPRa) via lentiviral infection[31] of MF-dCas9-MS2 cells and selected surviving cells after ferroptosis induction with RSL3, IKE, or tamoxifen in pools (see Supporting Methods).

Following expansion of surviving populations, we performed deep sequencing of guide RNAs and deconvolution using ENCoRE software[32] to generate a statistical index of enriched guides. The comparison of the corresponding highest-scoring candidate genes from all three conditions yielded a single gene, *Gch1* (Figure 1A, Table S1), with statistical confidence (RSL3, $p = 1.45 \times 10^{-4}$; IKE, $p = 7.20 \times 10^{-6}$; *Gpx4−/−*, $p = 0.0112$). As expected, we also observed substantial overlap between RSL3 (which inhibits GPX4 activity) and genetic deletion of *Gpx4*, identifying five additional shared ferroptotic protective genes among these conditions (*Ms4a15*, *Rpp25*, *BC048562*, *Tjp3*, *Egfl7*). IKE treatment (targeting system x_c^-) and *Gpx4$^{−/−}$* cells showed three enriched genes in common (*Fmnl1*, *Zfp933*, *Olfr147*); the IKE and RSL3 screens shared the target mitochondrial DNA topoisomerase I, *Top1mt*. As expected, *Gpx4* overexpression protected against RSL3 and IKE, but not against its own genetic deletion. We examined gene ontology (GO) term associations (Figure S1A) and performed ingenuity pathway analysis (Figure S1B) to explore functional commonalities. Both analyses confirmed the association of several pathways with ferroptosis. Among
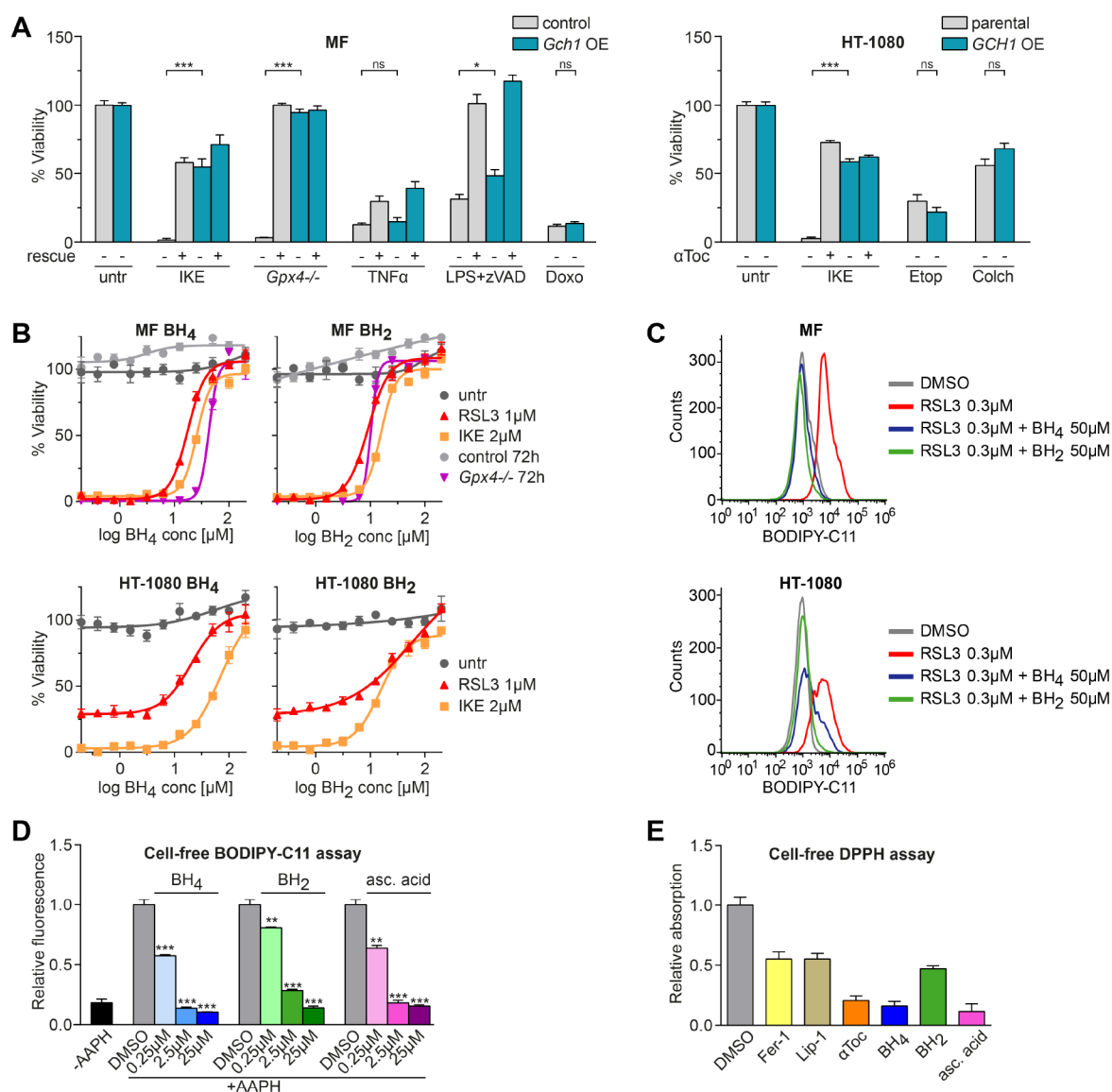
Figure 2. $Gch1$ overexpression and its downstream metabolites BH_4/BH_2 rescue from ferroptosis. (A) Survival of MF-dCas9-$Gch1$ ($Gch1$ OE) compared to empty vector MF control (control) cells and $GCH1$-IRES-Puro ($GCH1$ OE) cells compared to parental HT-1080 cells (parental), respectively, against inducers of cell death: Ferroptosis induced with 2 μM IKE and $Gpx4-/-$ by using 1 μM tamoxifen with 10 μM α-tocopherol (αToc) rescue. Extrinsic apoptosis induced by 20 ng/mL tumor necrosis factor α (TNFα) with 10 μM z-VAD-FMK (zVAD) rescue. Intrinsic apoptosis induced by 20 μM doxorubicin (Doxo), 25 μM etoposide (Etop), and 12.5 μM colchicine (Colch). Necroptosis induced by 1 μg/mL lipopolysaccharide (LPS) cotreatment with 10 μM zVAD with 10 μM necrostatin-1 (Nec-1) rescue. (B) Dose response curves of BH_2 and BH_4 starting at 200 μM rescuing from ferroptosis in MF control and parental HT-1080 cells induced by 1 μM RSL3, 2 μM IKE, and $Gpx4-/-$ by 1 μM tamoxifen. (C) Effect of BH_2 and BH_4 on lipid peroxidation induced by 0.3 μM RSL3 induction in MF control and parental HT-1080 cells measured by BODIPY 581/591 C11 stain (BODIPY-C11). A typical FACS histogram of $n = 4$ technical replicates of three independent repetitions is depicted. (D) Dose-dependent effect of BH_4, BH_2, and ascorbic acid (asc. acid) addition on BODIPY-C11 oxidation by 2,2′-azobis(2-methylpropionamidine) dihydrochloride (AAPH) in a cell-free system compared to DMSO control. (E) Antioxidative capacity of ferroptosis-relevant substances at equimolar concentration quantified by cell-free 2,2-diphenyl-1-picrylhydrazyl (DPPH) assay. Viability is plotted as mean ± SEM with at least duplicate (A) or $n = 4$ (B) technical replicates; three independent experiments were performed with similar results. Cell-free assays (D, E) are reported as mean ± SD of $n = 3$ technical replicates of three independent experiments with similar outcomes.

these, iron coordination and leukotriene biosynthesis are consistent with the current model of ferroptosis.

Next, we tested whether these candidate genes were robust regulators of ferroptosis. We generated 21 individual over-expressing MF cell pools and validated them in a viability assay against ferroptosis inducers. Doxorubicin, a DNA-intercalating agent that induces apoptosis, was included as a control for nonferroptotic cell death. Overexpression of several genes

($Gch1$, $Ms4a15$, $Rpp25$, $Olf r367$-ps, $L2hgdh$, $Slco1a6$, $Olfr39$) yielded almost complete protection against ferroptosis, comparable to α-tocopherol (Figure S1C, top). Others, including $Egfl7$, $Gpx4$, and $251009E07Rik$, were protective, albeit at modest levels under certain conditions (Figure S1C). Resistance correlated strongly among ferroptosis inducers but was largely absent for doxorubicin, supporting selectivity toward ferroptosis. Lipid peroxidation is a hallmark of
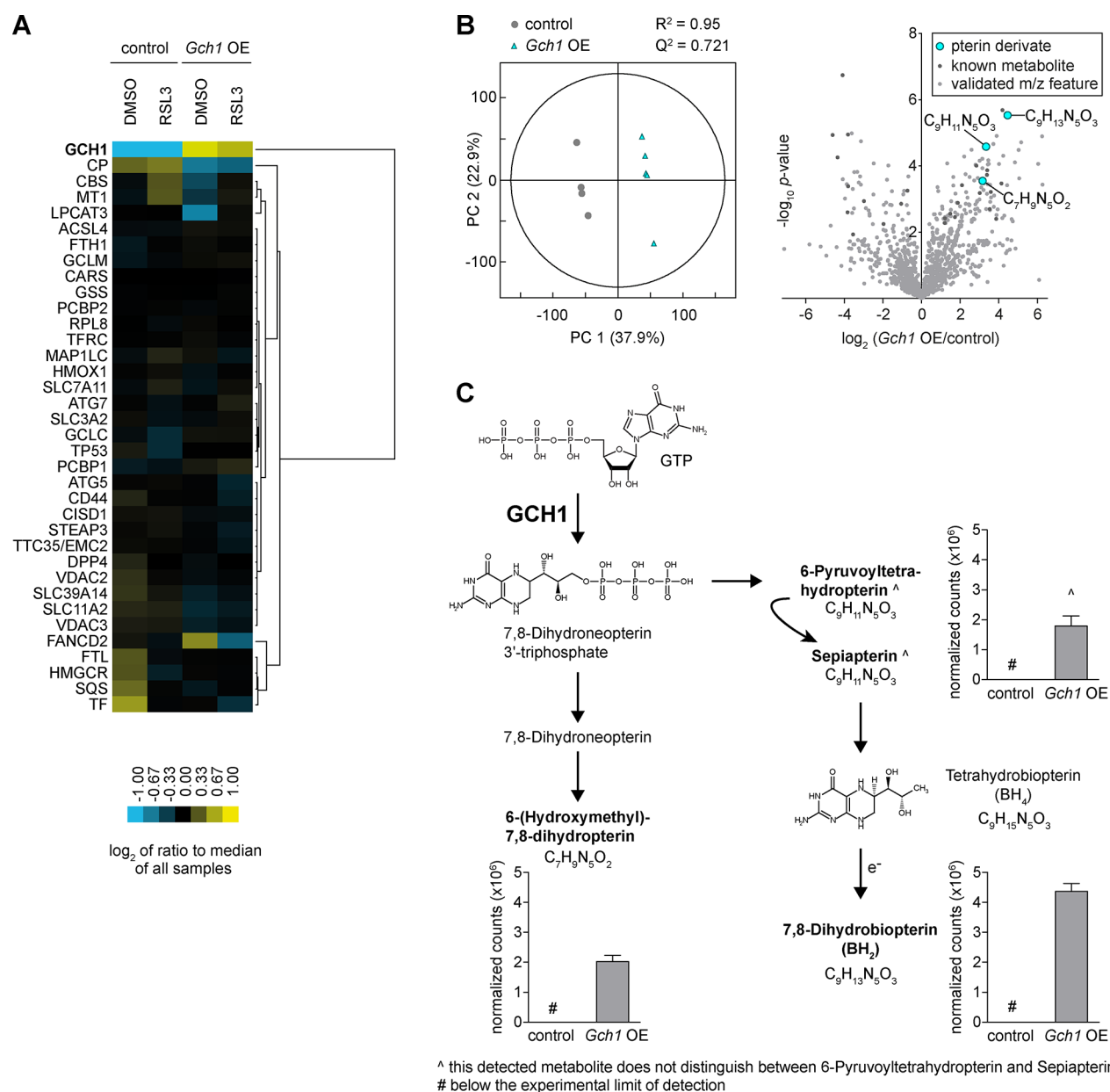
Figure 3. *Gch1* overexpression enhances folate pathway derivatives but does not affect known ferroptosis regulators. (A) Protein levels by heat map of known ferroptosis regulators upon 0.3 μM RSL3 treatment for 3 h in *Gch1*-overexpressing MF cells (*Gch1* OE) compared to control cells (control). Data were average of $n = 4$ or 5 independent biological replicates per condition. (B) Partial least-squares discriminant analysis of *Gch1* OE cells compared to control and volcano plot of whole-cell-shotgun metabolomics analysis. (C) Upregulated metabolic precursors of BH$_4$ and BH$_2$ in KEGG pathway of GCH1 in *Gch1* OE cells compared to control ($n = 5$ independent biological replicates).

ferroptosis; therefore, we assessed the extent of lipid peroxidation and cytosolic ROS using BODIPY 581/591 C11 (BODIPY-C11) and 2′,7′-dichlorodihydrofluorescein diacetate (DCF) as convenient proxies, followed later by lipidomic analysis (see below). Resistance to ferroptosis correlated with suppression of BODIPY-C11 oxidation. *Gch1*, *Ms4a15*, and *Olfr367 ps* overexpression virtually abolished oxidation of both the BODIPY-C11 and DCF sensors (Figure S1C, bottom). Thus, these genes function as novel and robust regulators of ferroptosis.

GCH1 Expression and Its Downstream Metabolites Determine Ferroptosis Resistance. Due to its shared presence under three screening conditions and robust protection, we focused our investigation on the role of *Gch1*

in ferroptosis. Pooled *Gch1*-overexpressing MF cells (*Gch1* OE) show a 6-fold increase in mRNA levels and were assayed in concentration-dependent survival against RSL3 challenge (Figure 1B). In agreement with the screening data, elevated *Gch1* expression rescued cells from up to 2 μM RSL3 treatment. We observed a comparable result in the ferroptosis-sensitive human fibrosarcoma cell line HT-1080 overexpressing a *GCH1*-IRES-Puro construct (*GCH1* OE), resulting in protection from RSL3 lethality (Figure 1C). Increased sensitivity to ferroptotic challenge was correspondingly observed upon stable CRISPRi-mediated[33] *Gch1* knockdown (*Gch1* KD) in MF cells (Figure S1D).

To ascertain whether *Gch1* is selectively relevant for ferroptosis or generally protective against cell death modalities,

we assayed lethal agents that work through diverse mechanisms. MF $Gch1$ OE cells were challenged with inducers of ferroptosis (IKE, $Gpx4$ deletion), extrinsic apoptosis (TNFα), intrinsic apoptosis (doxorubicin), or necroptosis (lipopolysaccharide + zVAD). $Gpx4$ ablation and IKE treatment resulted in complete viability loss in control cells, while $Gch1$ OE rescued $Gpx4$ ablation-induced death to >90%. Upregulation of $Gch1$ was incapable of protecting cells against inducers of apoptosis and only marginally effective against necroptosis, whereas zVAD and necrostatin-1 (Nec-1), respectively, potently inhibited these forms of cell death (Figure 2A, left panel). In line with this, human $GCH1$ OE HT-1080 cells were resistant to IKE-induced ferroptosis, but not the apoptosis-inducers etoposide and colchicine (Figure 2A, right panel). We therefore infer that $Gch1$ overexpression selectively counters ferroptotic cell death.

As GCH1 executes the rate-limiting biosynthesis step of pterins, including BH$_4$, $Gch1$ upregulation is expected to increase BH$_4$ concentrations. BH$_4$ is a critical cofactor for nitric oxide synthases (NOS enzymes). NOS uncoupling, primarily in vascular endothelium, is a state lacking BH$_4$ that generates superoxide instead of NO and therefore influences cellular redox status.[24] We first investigated whether NOS uncoupling affected ferroptotic cell death in MF cells. However, quantitative PCR of $Nos1-3$ and RNA sequencing revealed practically undetectable levels of enzyme transcripts independent of RSL3 treatment (Figure S2A,B). We confirmed these data by treating MF cells undergoing ferroptosis with diphenyleneiodonium (DPI), an inhibitor of NOS enzymes, and did not observe any protection in either MF control or $Gch1$ OE cells (Figure S2C). Thus, these results suggest that the role of BH$_4$ as an enzymatic cofactor of NOS enzymes does not affect ferroptosis resistance.

Some antioxidants, such as liproxstatin-1, ferrostatin-1, and vitamin E, can protect against lipid peroxidation. We analyzed whether BH$_4$ could act as a membrane-permeant antioxidant to influence ferroptosis sensitivity. To this end, we tested whether augmenting BH$_4$ levels was sufficient to protect against ferroptosis induced by chemical induction (RSL3 and IKE) or $Gpx4$ ablation. BH$_4$ supplementation in the culture medium prevented ferroptosis in a dose-dependent manner in MF cells induced by either stimulus (Figure 2B, top left). EC$_{50}$ values of BH$_4$ were 18 μM for RSL3, 26 μM for IKE, and 43 μM for $Gpx4-/-$ MF cells. A similar protective effect was seen in HT-1080 cells with an EC$_{50}$ of 21 μM for RSL3 and 69 μM for IKE (Figure 2B, bottom left). Independent treatment with BH$_2$ (7,8-dihydro-L-biopterin), a partially oxidized derivative of BH$_4$, augmented survival in a comparable fashion in both cell lines (Figure 2B, right panels). BH$_2$ EC$_{50}$ values were 9 μM for RSL3, 16 μM for IKE, and 10 μM for $Gpx4-/-$ in MF cells, and 59 μM for RSL3 and 15 μM for IKE in HT-1080 cells. Both compounds are reported to be plasma-membrane-permeable.[34] Peroxidized membrane phospholipids, consisting predominantly of 20 carbon ω-6 fatty acids, are substrates that drive cells toward ferroptosis. Using BODIPY-C11, we found that BH$_4$/BH$_2$ supplementation at 50 μM eliminated lipid peroxidation in RSL3-induced MF as well as HT-1080 cells (Figure 2C). We investigated the antioxidant characteristics of BH$_4$/BH$_2$ directly on cell-free oxidizable BODIPY-C11 treated with free-radical-producing 2,2′-azobis(2-methyl-propanimidamide) dihydrochloride (AAPH) and observed a dose-dependent decrease in oxidative fluorescence (Figure 2D) for BH$_4$, BH$_2$, and ascorbic acid. BH$_4$ has been reported to have

antioxidant scavenging activity. We therefore examined its reducing potential via cell-free 2,2-diphenyl-1-picrylhydrazyl (DPPH) assay. At equimolar concentrations, BH$_4$ has, together with ascorbic acid and α-tocopherol, the highest hydrogen-donating capacity compared to other ferroptosis inhibitors (Figure 2E). In total, these results show that the BH$_4$/BH$_2$ metabolites are potent antioxidants that strongly protect against ferroptotic cell death.

GCH1 Overexpression Does Not Affect Known Ferroptosis Regulators or the Glutathione System. We interrogated MF $Gch1$ OE cell lysates by protein mass spectrometry to determine if GCH1 overexpression would alter levels of known ferroptosis-related proteins (ferroptosis KEGG pathway).[2] Only one protein, the iron-carrier ceruloplasmin (CP), was counter-regulated with GCH1 and showed reduced levels in overexpressing cells, while 32 further ferroptosis-related proteins were not substantially altered in $Gch1$ OE cells (Figure 3A and Figure S3A).

Additionally, we analyzed glutathione, which is consumed during detoxification of lipid peroxides by the enzyme GPX4. To explore whether GCH1/BH$_4$/BH$_2$ has an effect on glutathione levels, we used the indicator dibromobimane, an indicator of free thiols (Figure S3B). Upon $Gch1$ over-expression, only a slight increase in free thiols/glutathione levels could be detected after L-buthionine-(S,R)-sulfoximine (BSO) treatment, while all other conditions including BH$_4$ supplementation were unchanged. This is in accordance with screening data following $Gpx4$ ablation, where glutathione is likely not consumed resolving lipid peroxides, and $Gch1$ OE still was able to fully protect from ferroptosis (Figure 1 and Figure S1). Hence, these data rule out a protective effect of GCH1 via the glutathione system.

Together, these data suggest an independent mechanism of ferroptosis protection by GCH1 relative to the known ferroptosis pathway proteins or the glutathione system.

GCH1 Overexpression Enhances the BH$_4$/BH$_2$ Folate Biosynthesis Pathway. We next investigated the consequences of $Gch1$ overexpression to the global cellular pool of metabolites by untargeted direct injection ESI-FT/ICR-MS metabolomics, a highly sensitive ultra-high-resolution semi-quantitative method that allows rapid and global profiling of metabolites, with the limitations that isobaric compounds cannot be discriminated. The whole-cell shotgun metabolite analysis delivered 1196 metabolites (Table S2), for which a global analysis using unsupervised techniques like hierarchical clustering and principal component analysis delivered very comparable metabolome profiles. We also applied supervised learning (partial least-squares discriminative analysis) and identified a distinct separation of control and $Gch1$-over-expressing cells within the first component (Figure 3B, left) caused by a robust increase in GCH1-derived pteridines from the folate biosynthesis pathway, most predominantly BH$_2$ (Figure 3B, right, and Figure 3C). 6-Hydroxymethyl-7,8-dihydropterin and 6-pyruvoyltetrahydropterin/sepiapterin with identical mass were also found to be increased (Figure 3C). We validated the effect of electrospray ionization and of cell lysis to the redox hemostasis of BH$_4$ and BH$_2$. We observed the formation of BH$_2$, the oxidation product of BH$_4$, over time (Figure S4A,B,D). After global screening, we developed a targeted UPLC-ToF-MS method for validation of the presence and identification of BH$_4$ and BH$_2$, separately (Figure S4C). Protein mass spectrometry in addition revealed a 5-fold increase in GCH1 protein in MF $Gch1$ OE cells (Figure 3A
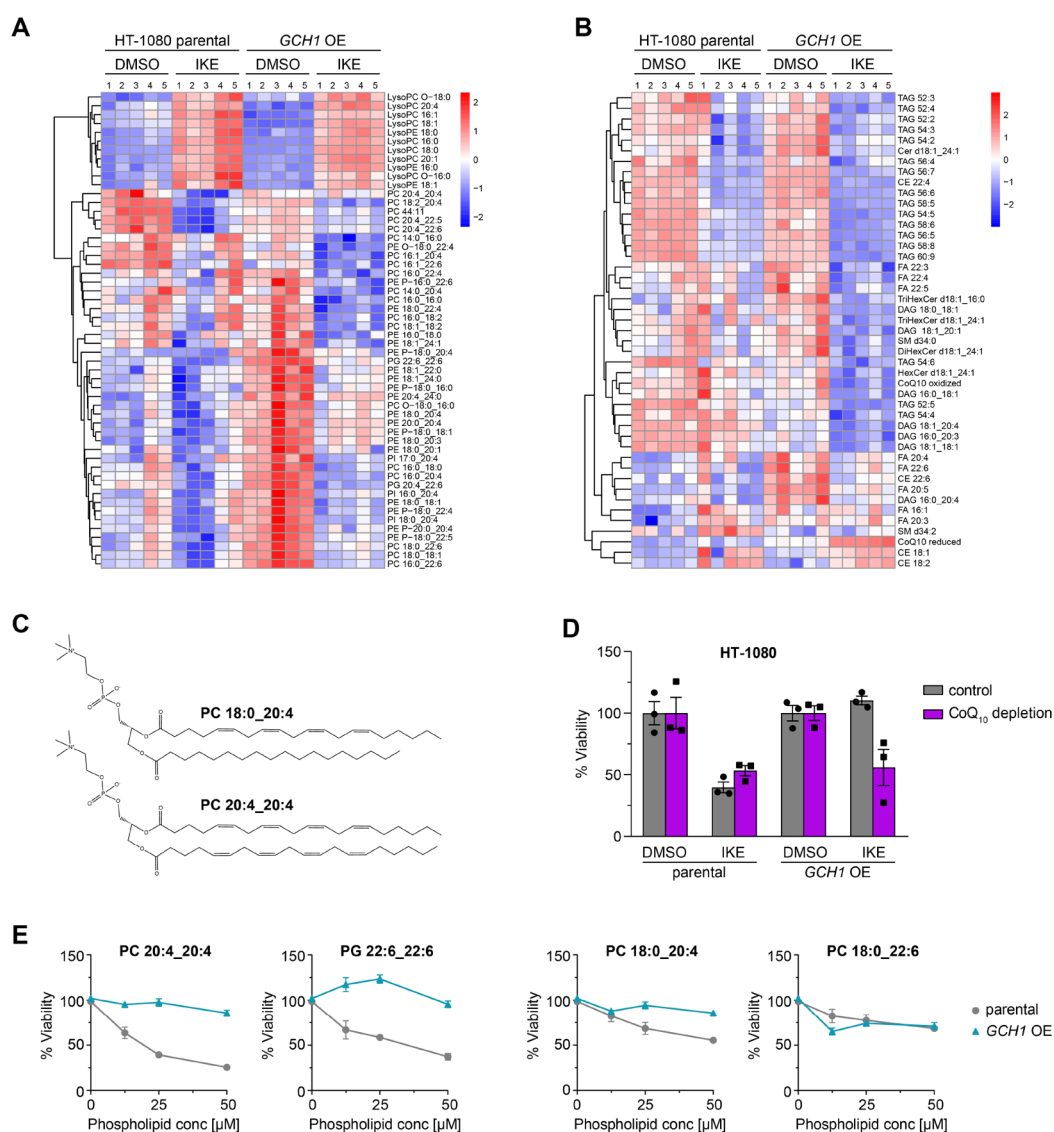
Figure 4. Untargeted lipidomics reveals *GCH1* overexpression cells protect from ferroptotic degradation of specific lipids. Heat map (one-way ANOVA; FDR-corrected *p*-value <0.05) showing changes in phospholipid profile (A), and glycerolipid, sphingolipid, and free fatty acid profiles (B) of DMSO or 10 μM IKE treated *GCH1*-overexpressing (*GCH1* OE) and parental HT-1080 cells. Each row represents Z-scored-normalized intensities of the differentiated lipid species. Each column represents the mean of $n = 2$ technical replicates of $n = 5$ independent biological replicates. The relative abundance of lipid is color-coded from red indicating high signal intensity to dark blue indicating low intensity and clustered using Pearson correlations. Abbreviations: PC, phosphatidylcholine; PE, phosphatidyl-ethanolamine; PI, phosphatidylinositol; PG, phosphatidylglycerol; LPC, lysoPC; LPE, LysoPE; PE P-, plasmalogen PE; PC/PE -O, ether-linked PE/PC; TAG, triacylglycerol; DAG, diacylglycerol; FA, fatty acid; CE, cholesterylester; CoQ$_{10}$, coenzyme Q$_{10}$; Cer, ceramide; HexCer, monohexosyl-Cer. (C) Line structure of representative phospholipids PC 18:0_20:4 with one saturated acyl chain and one polyunsaturated fatty acyl (PUFA) chain, as well as PC 20:4_20:4 with two PUFA chains. (D) Treatment of parental and *GCH1* OE HT-1080 cells with 4-nitrobenzoate in the absence of CoQ$_{10}$ with ferroptosis induction by 8 μM IKE. Viability is plotted as biological replicates $\pm$ SEM $n = 3$. (E) Treatment of parental and *GCH1* OE HT-1080 cells with exogenous PC 20:4_20:4, 18:0_20:4, 18:0_22:6, and PG 22:6_22:6 (concentrations 0−50 μM). Viability is plotted as mean $\pm$ SEM of $n = 4$ replicates.

and Figure S3A), demonstrating a stoichiometric relationship of metabolites to the rate-limiting enzyme GCH1.

Together, these data demonstrate that, as a consequence of increased cellular GCH1 levels, downstream products in the folate network, primarily the metabolites BH$_4$/BH$_2$, are selectively and strongly elevated, and they can act to suppress lipid peroxidation and ferroptotic cell death.

Untargeted Lipidomics Study Reveals that GCH1 Overexpression Selectively Protects Some PUFA-Phospholipids from Degradation. To investigate how *GCH1*

overexpression affects lipid composition and metabolism, we performed an untargeted mass-spectrometry-based lipidomics analysis on *GCH1*-overexpressing (*GCH1* OE) and parental HT-1080 cells treated with either 10 μM IKE or DMSO for 24 h. Unsupervised principal component analysis (PCA score plot) of extracted lipid features showed clear separation and tight clustering among the groups in both positive and negative electrospray ionization modes (Figure S5A,B).

The relative abundances of several lipid species were altered significantly (one-way ANOVA; FDR-corrected *p*-value <0.05)
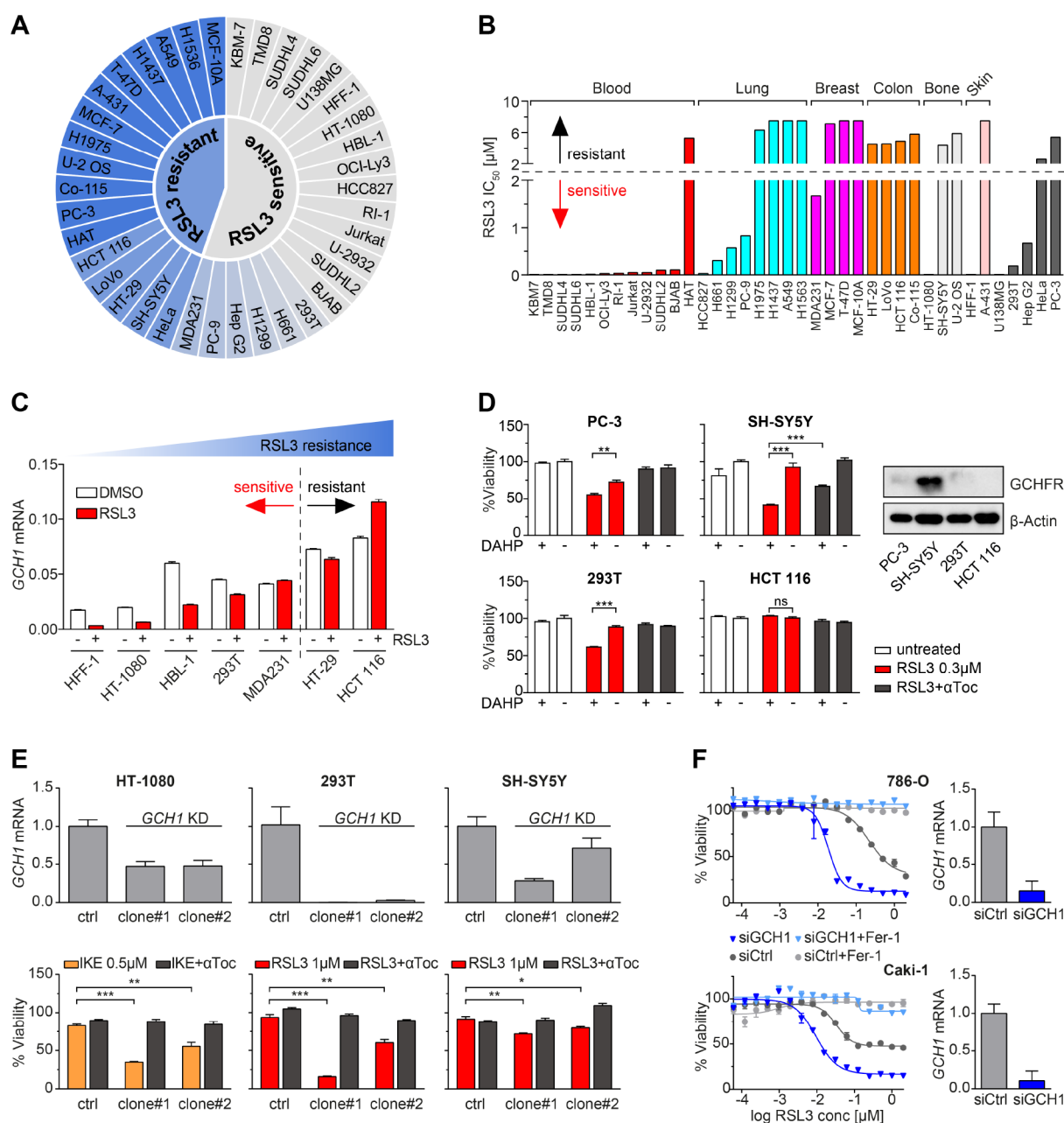
Figure 5. *GCH1* expression level determines cancer cell resistance to ferroptosis. (A) Color scaled profiling of 38 cancer cell lines according to RSL3 sensitivity based on their respective IC_{50}. (B) IC_{50} values of 38 cancer cell lines against RSL3, grouped by tissue of origin. (C) *GCH1* mRNA levels of seven representative cancer cell lines upon RSL3 treatment compared to DMSO. (D) Synthetic lethality induced by 1 mM DAHP and 0.3 μM RSL3 treatment in PC-3, SH-SY5Y, 293T, and HCT 116 cells with 10 μM αToc rescue. Protein levels of GCHFR compared to β-actin in these cell lines shown by Western blot. (E) *GCH1* mRNA levels and viability upon ferroptosis induction in HT-1080, 293T, and SH-SY5Y CRISPRi knockdown (*GCH1* KD) in two clonal cell lines each compared to respective empty vector control line (ctrl) with 10 μM αToc rescue. (F) *GCH1* mRNA levels and viability upon RSL3 treatment in 786-O and Caki-1 *GCH1* siRNA knockdown cells (siGCH1) compared to control siRNA (siCtrl) with 2 μM ferrostatin-1 (Fer-1) rescue. Viability is reported as mean $\pm$ SEM of $n = 3$ (D, E) or $n = 2$ (F) technical replicates. Relative mRNA expression is shown as mean $\pm$ SD of $n = 3$ technical replicates.

in response to IKE treatment in both groups, as expected (Table S3). We identified significant increases in the level of lysophosphatidylcholines (LysoPCs) and lysophosphatidyle-thanolamines (LysoPEs) and depletion of phospholipids mainly containing polyunsaturated fatty acyl (PUFA) chains, upon IKE treatment in both the parental and *GCH1* OE cells (Figure 4A). The accumulation of lysophospholipids, which are generated via a degradation reaction by enzymatic cleavage of the oxidized PUFA tail, has been reported upon treatment with ferroptosis inducers.[35] Degradation of phospholipids

containing arachidonic acid (e.g., PE 18:0_20:4), adrenic acid (e.g., PE 18:0_22:4), and docosahexaenoic acid (e.g., PC 18:0_22:6) was reported as a result of ferroptotic cell death.[3,35−37]

Triacylglycerols (TAGs) and diacylglycerols (DAGs), mostly found in lipid droplets, were also depleted upon IKE treatment in both the parental and *GCH1* OE cells (Figure 4B). Consistent with previous studies in cancer cell models, the TAGs that were depleted upon ferroptosis induction mostly contained PUFA tails.[37,38] These changes in the lipid
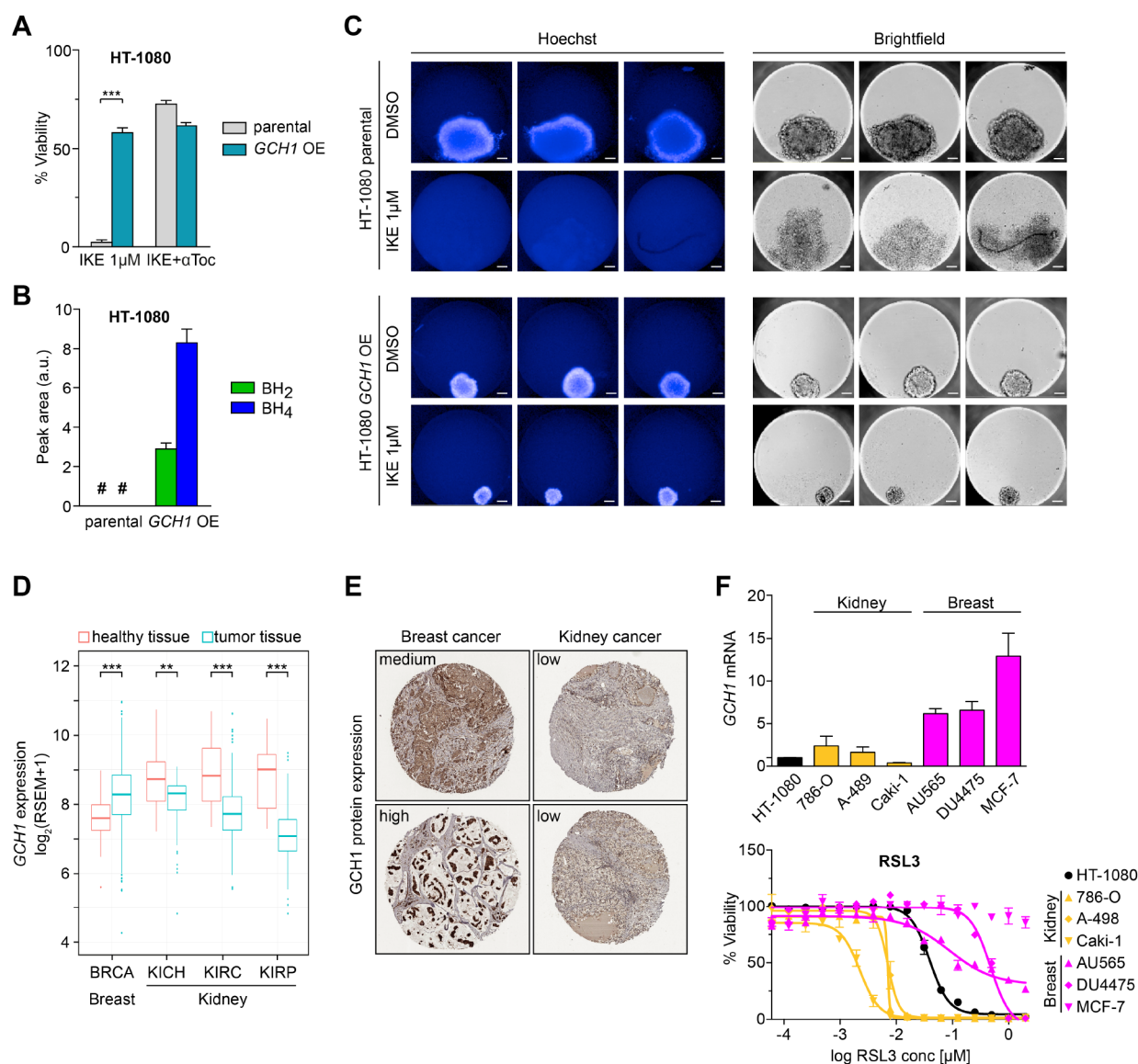
Figure 6. GCH1 expression increases resistance to ferroptosis in 3D spheroids, and human patient transcriptomics and pathology reveal coordinated GCH1 levels and ferroptosis sensitivity. (A) Data from Figure 2A showing survival of HT-1080 GCH1-overexpressing (GCH1 OE) cells against IKE-induced ferroptosis compared to parental cells (parental) with 10 μM αToc rescue. (B) BH$_4$ and BH$_2$ levels in HT-1080 GCH1 OE cells compared to parental cells of $n = 6$ biological replicates each. (C) Three-dimensional spheroid culture of GCH1 OE cells compared to parental cells and treatment with IKE. Three spheroids per condition were investigated. Scale bar = 100 μM. (D) GCH1 mRNA expression in tumor samples compared to healthy para-tumor tissue in breast and kidney cancers. BRCA, $p = 2.39 \times 10^{-17}$; KICH, $p = 0.02$; KIRC, $p = 7.54 \times 10^{-27}$; $p = $ KIRP, 10.7×10^{-25}. (E) GCH1 protein expression in breast and renal cancer tissue (Human Protein Atlas). (F) GCH1 mRNA and viability upon RSL3 treatment in kidney and breast cancer cell lines compared to HT-1080 cells. Viability is shown as mean $\pm$ SEM of $n = 2$ replicates of three independent repetitions of the experiment with similar outcomes. # means non detectable.

profile in both the parental and GCH1 OE cell lines surprisingly indicated sensitivity to ferroptotic degradation of lipids, even in GCH1 OE cells that are protected from dying. Thus, these results suggest that GCH1 overexpression, unlike GPX4, does not protect all PUFA−PLs from oxidative degradation but instead selectively prevents the oxidative degradation of specific PUFA−PLs that drive the execution of cell death during ferroptosis. This provided us with a unique opportunity to analyze the specific lipid peroxides that drive ferroptosis.

Intriguingly, we found that GCH1 OE cells selectively protected only an unusual and little-studied class of phosphatidylcholines with two PUFA chains, including PC 20:4_20:4, PC 20:4_20:5, and PC 20:4_22:6 from degradation upon IKE treatment (Figure 4A,C,E, and Figure S5D). Validating this result, we found that exogenous PC 20:4_20:4 or PG 22:6_22:6 treatment in the parental HT-1080 cells resulted in a greater sensitivity to IKE compared to the GCH1 OE cells (Figure 4C,E).

In contrast, depletion of the more common PCs with one PUFA tail and one saturated/monounsaturated fatty acyl chain after IKE treatment was observed even in the protected GCH1 OE cells, suggesting that degradation of these PC lipids does not specifically drive cell death (Figure 4A and Figure S5C). We also observed that single PUFA-containing phospholipids resulted in toxicity to the parental cells in a dose-dependent

manner (Figure 4E). The greater the number of bis-allylic sites, the more toxic the phospholipids were, likely due to their increased susceptibility to peroxidation. The *GCH1* OE cells were able to selectively protect the cells from phospholipids that had two PUFA tails. One-tail-PUFA containing lipids were less toxic to parental as well as *GCH1* OE cells (Figure 4E).

In addition, the lipid profile of the *GCH1* OE cells also showed a significant enrichment in reduced coenzyme Q_{10} (CoQ_{10}) levels after IKE treatment (Figure 4B and Figure S5E). This elevation of CoQ_{10} levels could be the result of the increased BH_4 in the cells, converting phenylalanine into tyrosine which can be further converted to 4-OH-benzoate, a precursor to CoQ_{10}. Under the oxidative stress induced by IKE treatment, the *GCH1* OE cells could be driving reduced CoQ_{10} biosynthesis, possibly also contributing to the protection of these from ferroptotic death. We observed that, when treated with 4-nitrobenzoate, an inhibitor of CoQ_{10} biosynthesis, in CoQ_{10}-depleted medium, *GCH1* OE cells were sensitized to IKE treatment, indicating that CoQ_{10} can also play a role in the protection of these cells from ferroptosis (Figure 4D and Figure S5C).

GCH1 Expression Level Determines Cancer Cell Resistance to Ferroptosis. Elevated GCH1 has been associated with increased tumorigenesis[28] and reduced survival in breast cancer patients.[39] In light of BH_4/BH_2-dependent protection, we examined if GCH1 determines ferroptosis sensitivity in cancer cell lines. We profiled 38 etiologically diverse cancer cell lines for RSL3 resistance, thereby benchmarking ferroptotic cell death IC_{50} for this substance in a dynamic concentration range still rescued by ferrostatin-1. Next, we classified these lines into categories "sensitive" or "resistant" by evaluating their specific lethality (IC_{50}) in RSL3-mediated ferroptosis: sensitive lines were lethal at doses <2 μM, while resistant lines remained vital at doses ≥2 μM (Figure 5A and Figure S6A). Further categorization by tissue of origin revealed a striking sensitivity of blood-derived tumors and widespread insensitivity in breast and colon tumors (Figure 5B and Figure S6A).

GCH1 expression is directly correlated to BH_4 levels.[40] Examination of *GCH1* mRNA levels after RSL3 induction from lines across the ferroptosis sensitivity range showed a linear relationship to ferroptosis resistance (Figure 5A,C). We additionally observed that *GCH1* transcripts were down-regulated following RSL3 stimulation in more sensitive cell lines (Figure 5C). In contrast, resistant cell lines did not substantially change *GCH1* mRNA levels over 6 h of treatment (Figure 5C); this suggests that *GCH1* mRNA can serve as a ferroptosis pharmacodynamic marker in ferroptosis-sensitive cells.

Next, to determine if cancer line resistance to ferroptosis could be attenuated via GCH1 activity modulation, we tested 2,4-diamino-6-hydroxypyrimidine (DAHP) in combination with RSL3. DAHP activates GCHFR, which then binds and inhibits GCH1. We tested cell lines with high (SH-SY5Y), low (PC-3 and 293T), and undetectable (HCT 116) levels of GCHFR (Figure 5D). Synthetic lethality was observed in cases where GCHFR was present (SH-SY5Y, PC-3, and 293T cells) but was absent in HCT 116 cells lacking GCHFR (Figure 5D). The level of lethality induced by RSL3/DAHP correlated to the level of the DAHP target, i.e., GCHFR. Consistent with this observation, CRISPRi-mediated knockdown of *GCH1* (*GCH1* KD) in the cell lines HT-1080, 293T, and SH-SY5Y significantly increased susceptibility of these lines to inducers

of ferroptotic cell death (Figure 5E and Figure S6B). Supplementation of either 100 μM BH_4 or BH_2 was sufficient to rescue *GCH1* KD viability completely (Figure S6B). Also, already sensitive renal cell lines 786-O and Caki-1 could be further sensitized to ferroptosis upon siRNA-mediated *GCH1* knockdown (siGCH1) (Figure 5F).

We further hypothesized that increased GCH1 enzymatic activity might have paracrine effects in cellular communities, as sensitivity to ferroptosis has been shown to have non-cell-autonomous aspects in previous studies.[22,34,41] Thus, we grew SH-SY5Y control donor cells with very high *GCH1* expression as well as *GCH1* knockdown (*GCH1* KD) donor SH-SY5Y cells (Figure 5D,E) at different densities and transferred their supernatants to recipient HT-1080 cells simultaneously challenged with IKE. Conditioned medium from high-*GCH1*-expressing SH-SY5Y control cells showed higher levels of BH_4 (Figure S7B) and was able to dose-dependently protect from ferroptosis, pointing to the potential of membrane-permeable BH_4 to protect neighboring cells in the microenvironment (Figure S7A).

Together, these data point to GCH1 expression and activity as a critical determinant of sensitivity to ferroptosis and that inhibition of GCH1 activity can sensitize resistant cancer cells to ferroptosis induction.

Higher GCH1 Levels Correlate to Ferroptosis Resistance in 3D Cultures. A direct correlation between GCH1 and cancer progression has been described.[27−29] We evaluated whether the GCH1/BH_4/BH_2 axis impacts ferroptosis sensitivity in a relevant oncogenic model. For this, we used the human HT-1080-*GCH1*-IRES-Puro (*GCH1* OE) line overexpressing *GCH1*, shown to be resistant to 1 μM IKE compared to parental HT-1080 cells (Figures 2B and 6A). Metabolomic evaluation of these cells by LC-MS/MS measurements confirmed a robust increase in BH_4/BH_2 pools (Figure 6B). We then used three-dimensional spheroid culture conditions. Notably, spheroids from *GCH1* OE HT-1080 were smaller in size but more compact, illuminated by stronger Hoechst staining. This indicates that *GCH1* over-expression leads to formation of denser three-dimensional structures. This finding indicates a likely more ferroptosis-protective environment in *GCH1* OE-derived spheroids due to their compact nature. Indeed, analysis of replicate experiments reproducibly showed complete loss of viability upon IKE treatment in parental HT-1080 spheroids, while substantial protection was observed in HT-1080 *GCH1* OE-derived spheroids (Figure 6C). This demonstrates that higher *GCH1* expression protects from ferroptosis also in a 3D spheroid environment.

Human Patient Transcriptomics and Pathology Reveal Coordinated *GCH1* Levels and Ferroptosis Sensitivity. To explore the relevance of GCH1-mediated ferroptosis resistance in clinical oncology we profiled RNaseq data from 6187 primary tumor biopsies from The Cancer Genome Atlas.[42] Patient samples from lung (LUAD), liver (LIHC), cervical (CESC), and colon (COAD) cancers showed particularly elevated *GCH1* levels (Figure S8), consistent with current and previously published data that breast, lung, and colon cancers are more resistant to ferroptosis[9] (Figure 5A,B). A mean difference in expression of ~16-fold was observed among all cancer types, substantially more than the 6-fold greater *Gch1* expression imparting complete protection in MF cells (Figures 1B and 2A).

Particularly striking are tumors of glioblastoma origin. Low-grade glioma (LGG) and glioblastoma multiforme (GBM) display dramatically reduced levels, approximately 8-fold less than colon tumors, and were the lowest of all cancer samples tested. This is consistent with pronounced sensitivity of the glioblastoma cell line U-138 MG to ferroptotic induction (Figure 5A).

Interestingly, tumors from breast cancer (BRCA) display significantly higher *GCH1* RNA expression compared to adjacent untransformed tissue (Figure 6D). In contrast, kidney cancers express significantly less *GCH1* than normal kidney tissue. These results demonstrate significant alterations in *GCH1* RNA expression between the tumor and the corresponding normal tissue. We also analyzed pathology samples from the Human Protein Atlas[43] for breast and kidney tumors and witnessed a marked difference between tissues with high GCH1 protein expression in breast cancer and almost no GCH1 protein in kidney sections (Figure 6E). Moreover, several breast cancer tumors appear to have condensed regions of high expression, which suggests consequences for a tumor microenvironment as observed in conditioned medium transfer experiments from SH-SY5Y to HT-1080 cells (Figure S7). In light of distinct expression differences in breast and kidney cells, we interrogated additional kidney (786-O, A-498, Caki-1) and breast-cancer-derived cell lines (AU565, DU4475, MCF-7). Strikingly, we observed tissue-dependent susceptibility to RSL3 treatment that correlated to the *GCH1* RNA expression level of each cell line (Figure 6F).

Together, the data show a correlation of tissue of origin *GCH1* levels with ferroptosis susceptibility, thereby introducing $GCH1/BH_4/BH_2$ as potential biomarkers for patient stratification in ferroptotic cancer treatment of distinct cancer types.

DISCUSSION

In this study, we found for the first time that the potent, endogenously produced antioxidants BH_4/BH_2 generated by the enzyme GCH1 can protect against ferroptosis in a GPX4-independent manner. *Gch1* was identified in a screen alongside several other genes (*Ms4a15, Rpp25, Olfr367 ps, L2hgdh, Slco1a6, Olfr39*) that protect robustly against the three ferroptosis inducers RSL3, IKE, and *Gpx4* deletion in individual overexpressing lines. During validation studies, other identified genes either showed lesser ferroptotic protection or protected only against individual stimuli. Reasons for these disparities may include gene silencing over time, selection against high expression, and mechanistic differences in protection. Accordingly, validation by clonal selection, as opposed to pooled lines used in this study, may yield singular, robustly protective lines. Strikingly, *GCH1* overexpression during screening and validation phases was highly consistent and demonstrates the power of CRISPRa to discover potent novel regulators of ferroptosis. It is nevertheless noteworthy that other protein components of the folate biosynthesis pathway were not identified in the screen, as they do not influence the rate-limiting step of BH_4 synthesis.

The breadth of factors identified in the whole genome screen is testament to the power of unbiased, genome-wide CRISPR activation. Two new reports published in parallel to this study revealed only a single ferroptosis-protective gene, AIFM2/FSP1, resulting from synthetic lethal and cDNA overexpression screens.[44,45] Notably, there are technical differences between the screens that account for the distinct outcomes. Sensitization knockout screens are likely to lack the dynamics of CRISPR overexpression screens, while cDNA libraries are rarely exhaustive; therefore, fewer genes were found in both recently published reports. On the other hand, AIFM2/FSP1 was not identified in our screen. Reasons for this may be (i) that the guides for AIFM2/FSP1 within the pooled library were insufficient for robust activation, (ii) that it may be mutated or silenced in the cells we studied, or (iii) that its guides may be underrepresented in the library, possibly because (iv) AIFM2/FSP1 is toxic or unfavorable for cells to express highly/constitutively.

Reactive oxygen species (ROS) are known to play an integral role in the development and pathological progression of cancer. Aberrant cellular division coupled with metabolic alterations shift the balance toward an increasingly ROS-driven environment.[13] Therefore, cells have established antioxidant mechanisms to counter ROS levels.[46] In this report, we have shown that *GCH1* expression elicits production of the potent antioxidants BH_4/BH_2, which when administered or produced endogenously can block lipid peroxidation and ferroptotic cell death. With an antioxidant capacity comparable to or stronger than liproxstatin-1, ferrostatin-1, and vitamin E, these potent metabolites can likely diffuse through membranes to neutralize reactive oxidative centers. Others have observed that radiation-induced skin damage generates free radicals, which are compensated by GCH1, NRF2, and BH_4.[47] Oxidative balance in macrophages is determined by GCH1,[48] and cardiac fibrosis and atrophy are reduced by supplemented BH_4.[24] Together, this suggests that $GCH1/BH_4/BH_2$ can act as a counterbalance to ROS load in cancer cells. Indeed, potent antioxidants decrease survival in mouse models and human cancer.[49]

GCH1 dictates levels of BH_4, and the presence of BH_4 leverages sensitivity to ferroptosis, emphasizing a direct correlation between the $GCH1/BH_4$ axis and ferroptosis inhibition. Proteins previously described to regulate ferroptotic signals as well as glutathione levels were not affected by *GCH1* overexpression (Figure 3A and Figure S3) implying that the antiferroptotic effect by $GCH1/BH_4$ is distinct from the previously described ferroptosis regulation pathways. Moreover, involvement of the glutathione antioxidant system is not necessary for survival. This is underscored by striking protection by *Gch1* overexpression in *Gpx4* knockout cells. Hence, GCH1 protects from ferroptotic cell death primarily through the antioxidant effect of BH_4/BH_2 and is entirely independent from GPX4-mediated ferroptosis protection.

Besides its robust antioxidant effect, the role of BH_4 as an enzymatic cofactor cannot definitively be ruled out by these studies. BH_4 interacts with iron in the catalytic core of several enzymes and binds directly to facilitate intermediate formation.[16] Of these, the most likely candidates to influence ferroptosis are the NOS enzymes, which were not substantially expressed or altered by NOS inhibitor addition (Figure S2). A possible role for lipid modulation exists via the BH_4-dependent enzyme AGMO; whether this occurs in human patients is unclear.[50] Protecting mitochondrial damage by antioxidants has been shown to increase mitochondrial metabolism, which may consume ferroptosis-sensitive fatty acids.[51]

An untargeted mass-spectrometry-based lipidomics analysis revealed that *GCH1* overexpression resulted in significant alterations in the lipid profiles upon IKE treatment. Interestingly, *GCH1* overexpression selectively protected PCs with two PUFA tails, which was confirmed through the addition of exogenous PCs to cells treated with IKE, resulting

in increased sensitivity only in parental HT-1080 cells. *GCH1*-overexpressing HT-1080 cells (*GCH1* OE) along with a parental line showed ferroptotic lipid signatures upon treatment of cells with IKE.[36−38] This suggests that *GCH1* overexpression and the presence of high BH$_4$ may not be enough to counter the oxidative degradation of several classes of lipids, including PUFA-containing TAGs and PLs. However, a small class of phospholipids are protected from oxidative damage in the *GCH1* OE HT-1080 cells, indicating that the fate of these phospholipids is predictive of the survival of the cell. *GCH1* OE HT-1080 cells were able to protect from basal toxicity resulting from lipid peroxation of PUFA more in the two-tailed PUFA PCs compared to the toxicity induced from the single-tailed PUFAs (Figure 4E). This suggests that the protection of these phospholipids from oxidative degradation is selective and can protect the cells from ferroptosis. We also observed a significant increase in reduced CoQ$_{10}$ (an antioxidant) in *GCH1* OE cells after IKE treatment, which could be the result of a high production of the CoQ$_{10}$ biosynthetic precursor 4-OH-benzoate. 4-OH-benzoate production is dependent on the BH$_4$-mediated conversion of phenylalanine to tyrosine, and both metabolites are upregulated (data not shown). These results suggest that, under oxidative stress, cells that have high BH$_4$ levels can synthesize CoQ$_{10}$ to alleviate oxidative damage. CoQ$_{10}$ was reported to be a critical second mechanism for ferroptosis protection.[44,45] Blocking *de novo* CoQ$_{10}$ synthesis after depleting CoQ$_{10}$ from the medium leads to sensitization of the *GCH1* OE HT-1080 cells to IKE treatment. This result suggests that the BH$_4$ can be used as a direct antioxidant to protect cells from lipid peroxidation or can be used for *de novo* synthesis of CoQ$_{10}$, which can also protect cells from ferroptosis. Apart from DAHP inhibition of enzymatic activity, this mechanism is unique in resensitizing *GCH1* OE cells to IKE treatment, and thus, the ability to synthesize *de novo* CoQ$_{10}$ may play a critical role in the protection of the cells from ferroptosis.

BH$_4$ can be secreted from cells.[34] Therefore, we compared survival of IKE-treated HT-1080 cells in conditioned medium from SH-SY5Y donor cells having high levels of GCH1 and observed a robust, donor-cell-number-dependent increase in survival of HT-1080 recipient cells (Figure S7). This implies that secreted BH$_4$/BH$_2$ or associated metabolites can help protecting neighboring cells from ferroptosis in a tumor microenvironment. This is of particular importance as few GCH1-overexpressing cells in a tumor may protect larger regions of the tumor from ferroptosis. In fact, sections from human breast cancer patients are suggestive of this phenomenon as not all cells within the tumor are expressing GCH1 at high levels but show individual collections of *GCH1* high-expressing cells (Figure 6E). Here, the high-expressing cells may conceivably protect the whole tumor from ferroptosis.

Our analysis of mRNA expression patterns of cancer patients pinpoint glioblastoma with prominently low *GCH1* expression levels, suggesting that these may be more susceptible to ferroptosis. In agreement with this, the tested cell line U-138 MG is markedly sensitive to RSL3. More profoundly, GCH1 determined glioblastoma tumor initiating capacity and patient survival in a clinically relevant study.[27] This is particularly relevant in light of clinical supplementation of BH$_4$ in patients with phenylalanine hydroxylase deficiency. Whether GCH1 contributes in oncology to a speculative intrinsic *in vivo*

ferroptosis mechanism is likely to be a subject of future interest.

Messenger RNA levels of *GCH1* correlate with the susceptibility to ferroptotic cell death (Figure 5C). Importantly, breast and kidney cells represent examples of cancers where tumor tissues differentially express *GCH1* when compared to their normal tissues. More precisely, breast cancer cells show elevated GCH1 protein in tumors, while kidney cells display reduced GCH1. In agreement, they are highly resistant and sensitive to ferroptosis, respectively. GCH1 has been reported to be associated with breast cancer incidence, progression, and survival times.[28] Hence, the GCH1/BH$_4$ axis may serve as a prognosticator of ferroptosis sensitivity and stratify patients for ferroptosis treatment in susceptible cancer cells. Certainly, whether intrinsic or exogenous, such hallmark antioxidants in tumors and under pathological conditions may serve as definitive clinical features for modulating cell survival *in vivo*.

■ ASSOCIATED CONTENT

ⓢ Supporting Information

The Supporting Information is available free of charge at https://pubs.acs.org/doi/10.1021/acscentsci.9b01063.

Additional data and figures including CRISPRa screening results, nitric oxide synthase data, GCH1 overexpression data, oxidation of BH$_4$ into BH$_2$ and identification of enhanced presence of BH$_4$, lipidomic analysis, extrinsic effect, and human patient *GCH1* levels (PDF)

Table S1: overexpression screen results (XLS)

Table S2: ESI-FT data (XLS)

Table S3: significant lipids (XLSX)

■ AUTHOR INFORMATION

Corresponding Authors

*E-mail: bstockwell@columbia.edu.
*E-mail: kamyar.hadian@helmholtz-muenchen.de.
*E-mail: joel.schick@helmholtz-muenchen.de.

ORCID ⓘ

Vanessa A. N. Kraft: 0000-0002-4432-7852
Stefanie M. Hauck: 0000-0002-1630-6827
Kamyar Hadian: 0000-0001-8727-2575
Joel A. Schick: 0000-0002-8623-4910

Author Contributions

◆V.A.N.K., C.T.B., and S.P. contributed equally to this work. Study initiation, K.H. and J.A.S.; conceptualization, B.R.S., K.H., and J.A.S.; methodology, V.A.N.K., C.T.B., S.P., L.R., C.M., F.Z., J.M.-P., X.B., N.A., J.K., S.B., J.D.D., B.R.S., K.H., and J.A.S.; investigation, V.A.N.K., C.T.B., S.P., L.R., C.M., F.Z., J.M.-P., X.B., N.A., J.K., S.B., and J.D.D.; data analysis, V.A.N.K., C.T.B., S.P., L.R., C.M., F.Z., J.M.-P., X.B., N.A., J.D.D., P.S.-K., S.M.H., B.R.S., K.H., and J.A.S.; writing, original draft, V.A.N.K., K.H., and J.A.S.; writing, review and editing, V.A.N.K., C.T.B., B.R.S., K.H., and J.A.S.; funding acquisition, B.R.S., K.H., and J.A.S.; resources: V.A.N.K., C.T.B., S.P., L.R., J.K., S.B., J.D.D., B.R.S., K.H., and J.A.S.; supervision, P.S.-K., S.M.H., B.R.S., K.H., and J.A.S.

Notes

The authors declare the following competing financial interest(s): B.R.S. holds equity in and consults with Inzen Therapeutics and is an inventor on patents and patent

applications related to IKE and ferroptosis. J.A.S. holds patents related to ferroptosis. The other authors declare no competing interests.

■ REFERENCES

(1) Dixon, S. J.; Lemberg, K. M.; Lamprecht, M. R.; Skouta, R.; Zaitsev, E. M.; Gleason, C. E.; Patel, D. N.; Bauer, A. J.; Cantley, A. M.; Yang, W. S.; et al. Ferroptosis: an iron-dependent form of nonapoptotic cell death. *Cell* **2012**, *149* (5), 1060.

(2) Stockwell, B. R.; Friedmann Angeli, J. P.; Bayir, H.; Bush, A. I.; Conrad, M.; Dixon, S. J.; Fulda, S.; Gascon, S.; Hatzios, S. K.; Kagan, V. E.; et al. Ferroptosis: A Regulated Cell Death Nexus Linking Metabolism, Redox Biology, and Disease. *Cell* **2017**, *171* (2), 273.

(3) Yang, W. S.; Stockwell, B. R. Ferroptosis: Death by Lipid Peroxidation. *Trends Cell Biol.* **2016**, *26* (3), 165.

(4) Conrad, M.; Kagan, V. E.; Bayir, H.; Pagnussat, G. C.; Head, B.; Traber, M. G.; Stockwell, B. R. Regulation of lipid peroxidation and ferroptosis in diverse species. *Genes Dev.* **2018**, *32* (9–10), 602.

(5) Maiorino, M.; Conrad, M.; Ursini, F. GPx4, Lipid Peroxidation, and Cell Death: Discoveries, Rediscoveries, and Open Issues. *Antioxid. Redox Signaling* **2018**, *29* (1), 61.

(6) Xie, Y.; Hou, W.; Song, X.; Yu, Y.; Huang, J.; Sun, X.; Kang, R.; Tang, D. Ferroptosis: process and function. *Cell Death Differ.* **2016**, *23* (3), 369.

(7) Gaschler, M. M.; Andia, A. A.; Liu, H.; Csuka, J. M.; Hurlocker, B.; Vaiana, C. A.; Heindel, D. W.; Zuckerman, D. S.; Bos, P. H.; Reznik, E.; et al. FINO2 initiates ferroptosis through GPX4 inactivation and iron oxidation. *Nat. Chem. Biol.* **2018**, *14* (5), 507.

(8) Shimada, K.; Skouta, R.; Kaplan, A.; Yang, W. S.; Hayano, M.; Dixon, S. J.; Brown, L. M.; Valenzuela, C. A.; Wolpaw, A. J.; Stockwell, B. R. Global survey of cell death mechanisms reveals metabolic regulation of ferroptosis. *Nat. Chem. Biol.* **2016**, *12* (7), 497.

(9) Yang, W. S.; SriRamaratnam, R.; Welsch, M. E.; Shimada, K.; Skouta, R.; Viswanathan, V. S.; Cheah, J. H.; Clemons, P. A.; Shamji, A. F.; Clish, C. B.; et al. Regulation of ferroptotic cancer cell death by GPX4. *Cell* **2014**, *156* (1–2), 317.

(10) Conrad, M.; Friedmann Angeli, J. P. Glutathione peroxidase 4 (Gpx4) and ferroptosis: what's so special about it? *Mol. Cell Oncol* **2015**, *2* (3), No. e995047.

(11) Friedmann Angeli, J. P.; Schneider, M.; Proneth, B.; Tyurina, Y. Y.; Tyurin, V. A.; Hammond, V. J.; Herbach, N.; Aichler, M.; Walch, A.; Eggenhofer, E.; et al. Inactivation of the ferroptosis regulator Gpx4 triggers acute renal failure in mice. *Nat. Cell Biol.* **2014**, *16* (12), 1180.

(12) Zilka, O.; Shah, R.; Li, B.; Friedmann Angeli, J. P.; Griesser, M.; Conrad, M.; Pratt, D. A. On the Mechanism of Cytoprotection by Ferrostatin-1 and Liproxstatin-1 and the Role of Lipid Peroxidation in Ferroptotic Cell Death. *ACS Cent. Sci.* **2017**, *3* (3), 232.

(13) Birben, E.; Sahiner, U. M.; Sackesen, C.; Erzurum, S.; Kalayci, O. Oxidative Stress and Antioxidant Defense. *World Allergy Organ. J.* **2012**, *5* (1), 9.

(14) Sullivan, L. B.; Chandel, N. S. Mitochondrial reactive oxygen species and cancer. *Cancer Metab* **2014**, *2*, 17.

(15) Gorrini, C.; Harris, I. S.; Mak, T. W. Modulation of oxidative stress as an anticancer strategy. *Nat. Rev. Drug Discovery* **2013**, *12* (12), 931.

(16) Werner, E. R.; Blau, N.; Thony, B. Tetrahydrobiopterin: biochemistry and pathophysiology. *Biochem. J.* **2011**, *438* (3), 397.

(17) Thony, B.; Auerbach, G.; Blau, N. Tetrahydrobiopterin biosynthesis, regeneration and functions. *Biochem. J.* **2000**, *347*, 1.

(18) Stuehr, D. J.; Griffith, O. W. Mammalian nitric oxide synthases. *Advances in enzymology and related areas of molecular biology* **2006**, *65*, 287.

(19) Tatham, A. L.; Crabtree, M. J.; Warrick, N.; Cai, S.; Alp, N. J.; Channon, K. M. GTP cyclohydrolase I expression, protein, and activity determine intracellular tetrahydrobiopterin levels, independent of GTP cyclohydrolase feedback regulatory protein expression. *J. Biol. Chem.* **2009**, *284* (20), 13660.

(20) Alp, N. J.; Mussa, S.; Khoo, J.; Cai, S.; Guzik, T.; Jefferson, A.; Goh, N.; Rockett, K. A.; Channon, K. M. Tetrahydrobiopterin-dependent preservation of nitric oxide-mediated endothelial function in diabetes by targeted transgenic GTP-cyclohydrolase I over-expression. *J. Clin. Invest.* **2003**, *112* (5), 725.

(21) Cai, S.; Khoo, J.; Channon, K. M. Augmented BH4 by gene transfer restores nitric oxide synthase function in hyperglycemic human endothelial cells. *Cardiovasc. Res.* **2005**, *65* (4), 823.

(22) Choi, H. J.; Jang, Y. J.; Kim, H. J.; Hwang, O. Tetrahydrobiopterin is released from and causes preferential death of catecholaminergic cells by oxidative stress. *Mol. Pharmacol.* **2000**, *58* (3), 633.

(23) Latremoliere, A.; Costigan, M. GCH1, BH4 and Pain. *Curr. Pharm. Biotechnol.* **2011**, *12* (10), 1728.

(24) Takimoto, E.; Champion, H. C.; Li, M.; Ren, S.; Rodriguez, E. R.; Tavazzi, B.; Lazzarino, G.; Paolocci, N.; Gabrielson, K. L.; Wang, Y.; et al. Oxidant stress from nitric oxide synthase-3 uncoupling stimulates cardiac pathologic remodeling from chronic pressure load. *J. Clin. Invest.* **2005**, *115* (5), 1221.

(25) Tegeder, I.; Costigan, M.; Griffin, R. S.; Abele, A.; Belfer, I.; Schmidt, H.; Ehnert, C.; Nejim, J.; Marian, C.; Scholz, J.; et al. GTP cyclohydrolase and tetrahydrobiopterin regulate pain sensitivity and persistence. *Nat. Med.* **2006**, *12*, 1269.

(26) Choi, H. J.; Lee, S. Y.; Cho, Y.; No, H.; Kim, S. W.; Hwang, O. Tetrahydrobiopterin causes mitochondrial dysfunction in dopaminergic cells: implications for Parkinson's disease. *Neurochem. Int.* **2006**, *48* (4), 255.

(27) Tran, A. N.; Walker, K.; Harrison, D. G.; Chen, W.; Mobley, J.; Hocevar, L.; Hackney, J. R.; Sedaka, R. S.; Pollock, J. S.; Goldberg, M. S.; et al. Reactive species balance via GTP cyclohydrolase I regulates glioblastoma growth and tumor initiating cell maintenance. *Neuro-oncology* **2018**, *20* (8), 1055.

(28) Pickert, G.; Lim, H. Y.; Weigert, A.; Haussler, A.; Myrczek, T.; Waldner, M.; Labocha, S.; Ferreiros, N.; Geisslinger, G.; Lotsch, J.; et al. Inhibition of GTP cyclohydrolase attenuates tumor growth by reducing angiogenesis and M2-like polarization of tumor associated macrophages. *Int. J. Cancer* **2013**, *132* (3), 591.

(29) Cronin, S. J. F.; Seehus, C.; Weidinger, A.; Talbot, S.; Reissig, S.; Seifert, M.; Pierson, Y.; McNeill, E.; Longhi, M. S.; Turnes, B. L.; et al. The metabolite BH4 controls T cell proliferation in autoimmunity and cancer. *Nature* **2018**, *563*, 564.

(30) Mannes, A. M.; Seiler, A.; Bosello, V.; Maiorino, M.; Conrad, M. Cysteine mutant of mammalian GPx4 rescues cell death induced

by disruption of the wild-type selenoenzyme. *FASEB J.* **2011**, *25* (7), 2135.

(31) Konermann, S.; Brigham, M. D.; Trevino, A. E.; Joung, J.; Abudayyeh, O. O.; Barcena, C.; Hsu, P. D.; Habib, N.; Gootenberg, J. S.; Nishimasu, H.; et al. Genome-scale transcriptional activation by an engineered CRISPR-Cas9 complex. *Nature* **2015**, *517* (7536), 583.

(32) Trumbach, D.; Pfeiffer, S.; Poppe, M.; Scherb, H.; Doll, S.; Wurst, W.; Schick, J. A. ENCoRE: an efficient software for CRISPR screens identifies new players in extrinsic apoptosis. *BMC Genomics* **2017**, *18* (1), 905.

(33) Qi, L. S.; Larson, M. H.; Gilbert, L. A.; Doudna, J. A.; Weissman, J. S.; Arkin, A. P.; Lim, W. A. Repurposing CRISPR as an RNA-guided platform for sequence-specific control of gene expression. *Cell* **2013**, *152* (5), 1173.

(34) Walter, R.; Schaffner, A.; Blau, N.; Kierat, L.; Schoedon, G. Tetrahydrobiopterin is a secretory product of murine vascular endothelial cells. *Biochem. Biophys. Res. Commun.* **1994**, *203* (3), 1522.

(35) Skouta, R.; Dixon, S. J.; Wang, J.; Dunn, D. E.; Orman, M.; Shimada, K.; Rosenberg, P. A.; Lo, D. C.; Weinberg, J. M.; Linkermann, A.; et al. Ferrostatins inhibit oxidative lipid damage and cell death in diverse disease models. *J. Am. Chem. Soc.* **2014**, *136* (12), 4551.

(36) Kagan, V. E.; Mao, G.; Qu, F.; Angeli, J. P.; Doll, S.; Croix, C. S.; Dar, H. H.; Liu, B.; Tyurin, V. A.; Ritov, V. B.; et al. Oxidized arachidonic and adrenic PEs navigate cells to ferroptosis. *Nat. Chem. Biol.* **2017**, *13* (1), 81.

(37) Zhang, Y.; Tan, H.; Daniels, J. D.; Zandkarimi, F.; Liu, H.; Brown, L. M.; Uchida, K.; O'Connor, O. A.; Stockwell, B. R. Imidazole Ketone Erastin Induces Ferroptosis and Slows Tumor Growth in a Mouse Lymphoma Model. *Cell chemical biology* **2019**, *26* (5), 623.

(38) Zou, Y.; Palte, M. J.; Deik, A. A.; Li, H.; Eaton, J. K.; Wang, W.; Tseng, Y. Y.; Deasy, R.; Kost-Alimova, M.; Dancik, V.; et al. A GPX4-dependent cancer cell state underlies the clear-cell morphology and confers sensitivity to ferroptosis. *Nat. Commun.* **2019**, *10* (1), 1617.

(39) Chen, L.; Zeng, X.; Kleibeuker, E.; Buffa, F.; Barberis, A.; Leek, R. D.; Roxanis, I.; Zhang, W.; Worth, A.; Beech, J. S.; et al. Paracrine effect of GTP cyclohydrolase and angiopoietin-1 interaction in stromal fibroblasts on tumor Tie2 activation and breast cancer growth. *Oncotarget* **2016**, *7* (8), 9353.

(40) Harada, T.; Kagamiyama, H.; Hatakeyama, K. Feedback regulation mechanisms for the control of GTP cyclohydrolase I activity. *Science (Washington, DC, U. S.)* **1993**, *260* (5113), 1507.

(41) Linkermann, A.; Skouta, R.; Himmerkus, N.; Mulay, S. R.; Dewitz, C.; De Zen, F.; Prokai, A.; Zuchtriegel, G.; Krombach, F.; Welz, P. S.; et al. Synchronized renal tubular cell death involves ferroptosis. *Proc. Natl. Acad. Sci. U. S. A.* **2014**, *111* (47), 16836.

(42) TCGA, TCGA Research Network. https://www.cancer.gov/tcga.

(43) Uhlen, M.; Zhang, C.; Lee, S.; Sjostedt, E.; Fagerberg, L.; Bidkhori, G.; Benfeitas, R.; Arif, M.; Liu, Z.; Edfors, F. A pathology atlas of the human cancer transcriptome. *Science (Washington, DC, U. S.)* **2017**, *357* (6352), eaan2507.

(44) Bersuker, K.; Hendricks, J.; Li, Z.; Magtanong, L.; Ford, B.; Tang, P. H.; Roberts, M. A.; Tong, B.; Maimone, T. J.; Zoncu, R. The CoQ oxidoreductase FSP1 acts parallel to GPX4 to inhibit ferroptosis. *Nature* **2019**, *575*, 688.

(45) Doll, S.; Freitas, F. P.; Shah, R.; Aldrovandi, M.; da Silva, M. C.; Ingold, I.; Grocin, A. G.; Xavier da Silva, T. N.; Panzilius, E.; Scheel, C. FSP1 is a glutathione-independent ferroptosis suppressor. *Nature* **2019**, *575*, 693.

(46) Kumari, S.; Badana, A. K.; G, M. M.; G, S.; Malla, R. Reactive Oxygen Species: A Key Constituent in Cancer Survival. *Biomarker Insights* **2018**, *13*, 117727191875539.

(47) Xue, J.; Yu, C.; Sheng, W.; Zhu, W.; Luo, J.; Zhang, Q.; Yang, H.; Cao, H.; Wang, W.; Zhou, J.; et al. The Nrf2/GCH1/BH4 Axis Ameliorates Radiation-Induced Skin Injury by Modulating the ROS Cascade. *J. Invest. Dermatol.* **2017**, *137* (10), 2059.

(48) McNeill, E.; Crabtree, M. J.; Sahgal, N.; Patel, J.; Chuaiphichai, S.; Iqbal, A. J.; Hale, A. B.; Greaves, D. R.; Channon, K. M. Regulation of iNOS function and cellular redox state by macrophage Gch1 reveals specific requirements for tetrahydrobiopterin in NRF2 activation. *Free Radical Biol. Med.* **2015**, *79*, 206.

(49) Sayin, V. I.; Ibrahim, M. X.; Larsson, E.; Nilsson, J. A.; Lindahl, P.; Bergo, M. O. Antioxidants accelerate lung cancer progression in mice. *Sci. Transl. Med.* **2014**, *6* (221), 221ra15.

(50) Vilaseca, M. A.; Lambruschini, N.; Gomez-Lopez, L.; Gutierrez, A.; Moreno, J.; Tondo, M.; Artuch, R.; Campistol, J. Long-chain polyunsaturated fatty acid status in phenylketonuric patients treated with tetrahydrobiopterin. *Clin. Biochem.* **2010**, *43* (4−5), 411.

(51) Purushothaman, S.; Nair, R. R. Mitoprotective antioxidant EUK-134 stimulates fatty acid oxidation and prevents hypertrophy in H9C2 cells. *Mol. Cell. Biochem.* **2016**, *420* (1−2), 185.